Supplemental material: Supplemental material: Final COMPASS results on the transverse-spin-dependent azimuthal asymmetries in the pion-induced Drell-Yan process

COMPASS Collaboration[1]

[1] *CERN, 1211 Geneva 23, Switzerland*

This supplemental material includes additional information on the higher-twist asymmetries, a comparison of the new results with our previous publication [1], a comparison of the results from the extended (4.0 GeV/$c^2 <$ $M_{\mu\mu}$ $<$9.0 GeV/c^2) and the previously used (4.3 GeV/$c^2 <$ $M_{\mu\mu}$ $<$8.5 GeV/c^2) mass ranges, as well as additional information about the background fraction and kinematic distributions.

In Fig. 1, the combined 2015 and 2018 COMPASS results obtained for the two subleading-twist TSAs $A_T^{\sin(\varphi_{CS}+\varphi_S)}$ and $A_T^{\sin(\varphi_{CS}-\varphi_S)}$ are shown as a function of the variables x_N, x_π, x_F, q_T and $M_{\mu\mu}$. Compared to the twist-2 TSAs, the statistical uncertainties of both higher-twist TSAs are larger, which is explained by the relative smallness of the associated depolarization factor. The asymmetries are consistent with zero within one standard deviation of the total uncertainty. The asymmetry $A_T^{\sin(\varphi_{CS}-\varphi_S)}$ tends to be positive in all kinematic sub-ranges covered by the measurement.

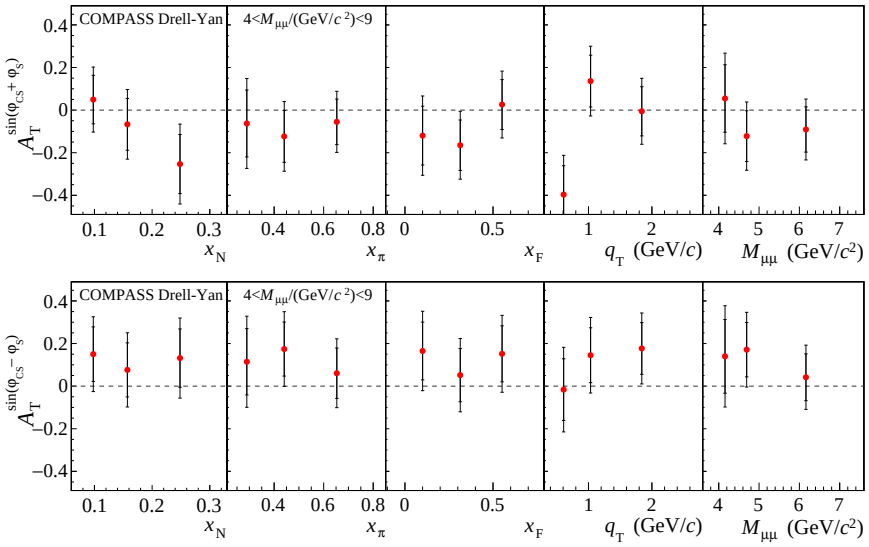

FIG. 1. Combined 2015 and 2018 results on the kinematic dependences of the higher-twist TSAs. Inner (outer) error bars represent statistical (total experimental) uncertainties.

In Fig. 2 the results for all five extracted TSAs integrated over the entire kinematic range are shown. The most significant effect is measured for the transversity TSA, $A_T^{\sin(2\varphi_{CS}-\varphi_S)}$.

In Fig. 3 the invariant mass spectrum measured by COMPASS is shown together with the pure Drell-Yan contribution evaluated using the COMPASS Monte-Carlo simulation chain. The red histogram, obtained by subtracting the Drell-Yan MC distribution from the measured spectrum, illustrates the overall background contribution originating from charmonia, semi-muonic open-charm decays and combinatorial background from uncorrelated opposite-sign muons. The background fraction as a function of mass was parameterised using an exponential fit on the background distributions. The procedure was verified for all kinematic bins using alternative methods for background evaluation, leading to very close results (e.g. fitting the mass distribution in the background-free intervals 6.0 GeV/$c^2 <$ $M_{\mu\mu}$ $<$8.5 GeV/c^2 using exponential functions or Chebyshev polynomials and then extrapolating the obtained curves to lower masses to determine the background fraction). In Fig. 4 the evaluated background fraction is shown as a function of kinematic variables.

In Fig. 5 shows the combined 2015 and 2018 results, obtained for the extended mass range 4.0 GeV/$c^2 <$ $M_{\mu\mu}$ $<$9.0 GeV/c^2as presented in this letter, in comparison to the TSAs extracted with the narrower mass range

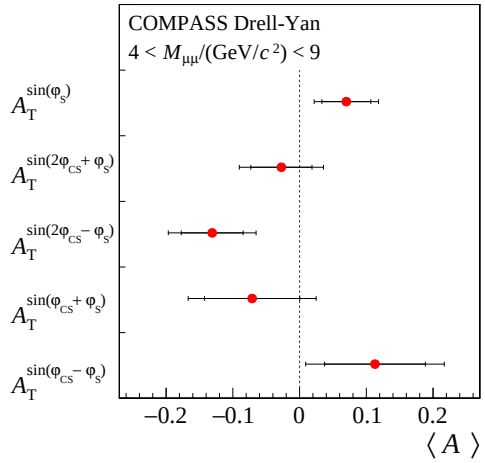

FIG. 2. Extracted twist-2 and higher-twist Drell-Yan TSAs. Inner (outer) error bars represent statistical (total experimental) uncertainties.

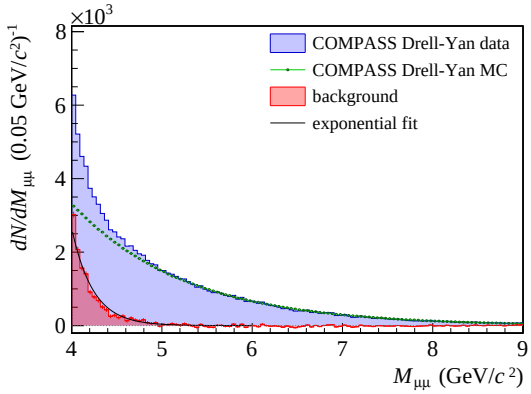

FIG. 3. The dimuon invariant mass distribution from reconstructed events in the mass range selected for the analysis (blue histogram) is compared to the normalised distribution of Drell-Yan events from a COMPASS Monte-Carlo simulation (green histogram). The difference between the two histograms corresponds to the background events and is shown by the red histogram. The background distribution is fitted by an exponential curve (black line).

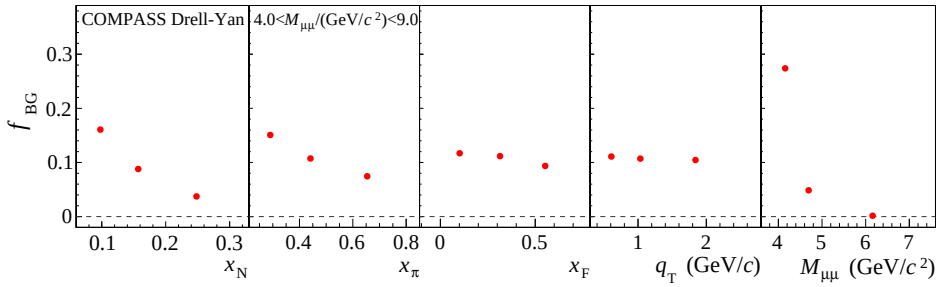

FIG. 4. Estimated background fraction in different kinematic bins.

4.3 GeV/$c^2 < M_{\mu\mu} <$ 8.5 GeV/c^2. The two sets of data points are seen to be consistent. The results from the extended mass range have noticeably smaller uncertainties. In Fig. 6 our new measurements are compared to the previously published results, which were based on 2015 data only [1]. Note that since 2017 the 2015 data was re-processed using improved reconstruction settings, detector alignment and calibrations, etc. The new results, which demonstrate the much higher statistical precision, supersede those of the first publication.

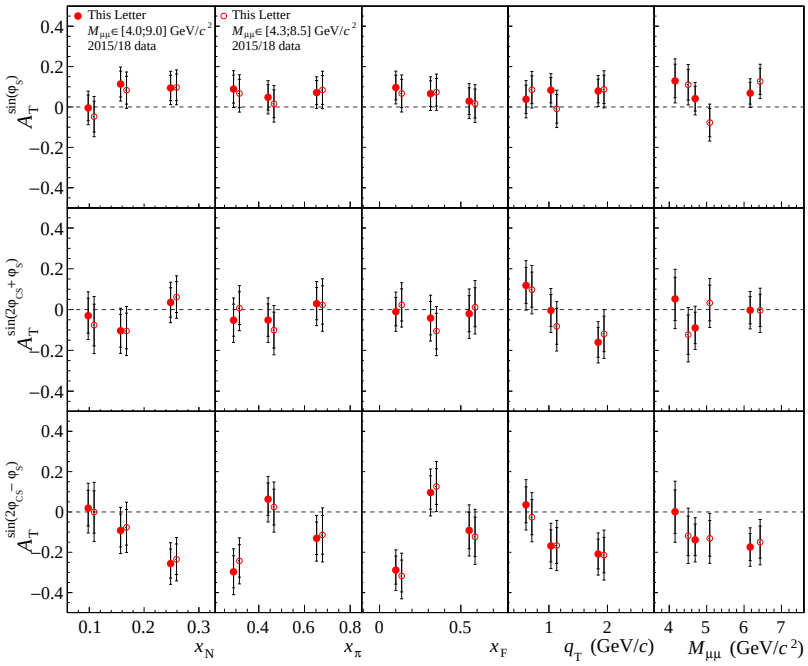

FIG. 5. Combined 2015 and 2018 results on the kinematic dependences of the Sivers, pretzelosity, and transversity TSAs (top to bottom) from the new measurement using the extended mass range 4.0 GeV/$c^2 < M_{\mu\mu} <$ 9.0 GeV/c^2 (filled circles) are compared with the results obtained for the narrower mass range 4.3 GeV/$c^2 < M_{\mu\mu} <$ 8.5 GeV/c^2 (empty circles). Inner (outer) error bars represent statistical (total experimental) uncertainties. The empty circles are artificially staggered w.r.t. the filled circles for better visibility. For the $M_{\mu\mu}$-dependence the original position is kept for both sets of points.

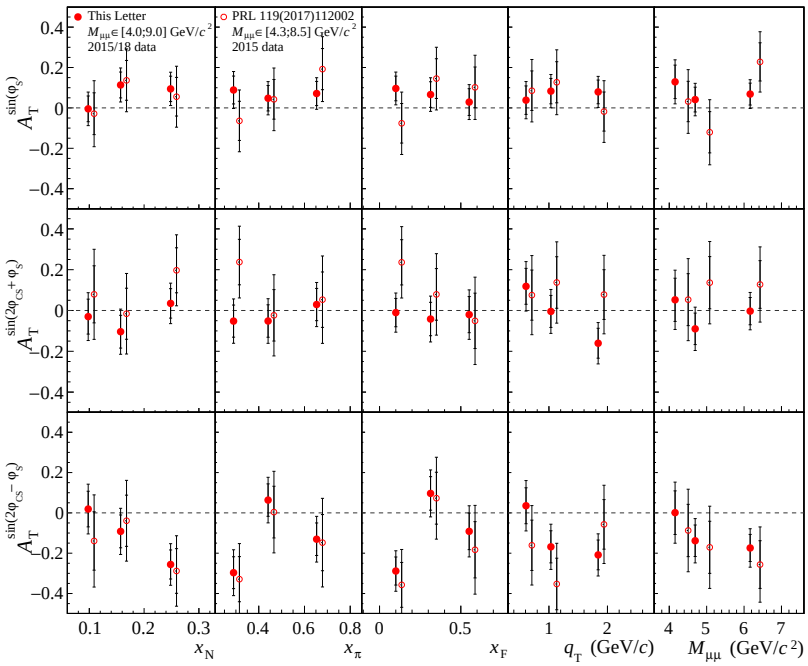

FIG. 6. The combined 2015 and 2018 results on the kinematic dependences of the Sivers, pretzelosity, and transversity TSAs (top to bottom) from the new measurement (filled circles) are compared with the results from the previous publication obtained with 2015 data only (empty circles) [1]. The new results were obtained with the extended mass range (4.0 GeV/$c^2 <$ $M_{\mu\mu} <$ 9.0 GeV/c^2), while for the previous ones a narrower mass interval (4.3 GeV/$c^2 <$ $M_{\mu\mu} <$ 8.5 GeV/c^2) was used. Otherwise as in Fig. 5

[1] M. Aghasyan *et al.* (COMPASS collaboration), Phys. Rev. Lett. **119**, 112002 (2017), arXiv:1704.00488 [hep-ex].